# In-situ Electrical Resistance Measurements for Soldering Studies in Hybrid AM

Alexander P. Pustinger, Joselin Corral, Arianna Villegas, David Espalin

The University of Texas at El Paso, W.M. Keck Center for 3D Innovation, El Paso, Texas

*Keywords: Hybrid AM, 4-wire resistance measurements, encapsulation, laser soldering*



## Abstract

The convergence of additive manufacturing (AM) along with multiple applicable technologies has been shown to augment the functionality of printed parts such that mechanical, electrical, and electromagnetic functions can, for example, reside within the same part. This work used an electrical connector commonly used in satellites to demonstrate a hybrid AM approach by embedding the connector, ultrasonically embedding wires, and laser soldering. The connector was a six-pin Easy-on FFC/FPC connector with a fine pitch and leads of 200-micron width. Resistance measurements were carried out during laser soldering, application of insulation material, and encapsulation with thermoplastic extruded at high temperatures (> 300ºC). The measurements were made to observe the impact of 1) a laser power profile and 2) thermal input from the extrusion nozzle and heated build environment for diagnostics of low yield or performance. Additionally, temperature history data was collected to coincide with resistance measurements.

## Introduction

The interest in hybrid additive manufacturing (hybrid AM) for on-orbit production has grown due to its potential to fabricate a wide range of devices, such as small satellites and space station electronics, using a single manufacturing system. This approach offers the advantage of reducing the need for on-orbit spare part inventory. Of particular significance is the fabrication of electronics on orbit, which is relevant in both terrestrial and on-orbit scenarios. Examples of on-orbit fabrication exist both with and without the utilization of AM. For instance, COSM Advanced Manufacturing Systems LLC made significant progress in improving an electron gun, optics, and beam control for in-space assembly using the Electron Beam Free Form Fabrication method. This technique employs E-beams to additively manufacture metal parts for the aerospace industry [Bowman, 2018]. Another example involves the use of deployable structures and on-orbit direct write printing to enhance Supervised Autonomous Assembly (SAA), an approach that promotes autonomous assembly and efficiency in AM without requiring a system operator [Grande, 2021]. In contrast, a non-AM example demonstrates the use of pre-manufactured components assembled

for on-orbit manufacturing, supporting various operations involved in the design of spacecraft assembly on orbit [Doris, 2018].

Despite the notable achievements in on-orbit fabrication, the research focus on printing electronics on-orbit has been limited. To the best of the author's knowledge, automated hybrid AM has not been utilized for on-orbit electronics fabrication. Therefore, this study aims to fabricate coupons containing components and materials relevant to space applications. These coupons will serve as a baseline for future comparisons with on-orbit or similar environment experiments. Although the fabrication process did not take place on-orbit or in space-like conditions, it considered the potential challenges posed by gravity and vacuum. Before exploring these challenges, a brief overview of 3D electronics and laser soldering will be provided.

The utilization of interconnects and conductive materials in AM has progressed to simplify assembly complexity and reduce redundant mass/packaging size. A collaborative effort between NASA/GRC (National Aeronautics and Space Administration/Glenn Research Center) and America Makes resulted in the development of an AM process than embeds interconnects within a hybrid AM process, combining vat photopolymerization (VPP) and direct printing [Liu, 2019]. In their approach, a pressure sensor was fabricated, incorporating VPP-fabricated insulated structures and interconnects created through direct dispensing. By depositing a layer of photocurable material on top, they achieved a fully encapsulated circuit. Other studies have explored the integration of interconnects into flexible materials to create stretchable electronics for applications in soft robotics [Ladd, 2016]. This involved using a syringe extrusion-based 3D printing process with conductive silicone to manufacture a functional game dice with an embedded accelerometer. Additionally, the Aerosol Jet Printing Method was employed in another example, where silver-based ink was deposited onto a PLA prosthetic to create strain gauge sensors [Lu, 2018]. In addition to interconnects, various literature sources have described the use of connectors within AM parts, including SMA connectors [Shemelya, 2015], SMA, coaxial SMA, and N-type connectors [Hao, Yu, Liang, Shemelya, 2018], N-type Coaxial and N-type connectors [Liang, Yu, Shemelya, MacDonald, Xin, 2015], and microUSB connectors [Shemelya, 2015]. Alongside interconnectors and connectors, the quality of the joints between them is crucial for the proper functioning of circuits.

To implement laser soldering technology effectively, it is crucial to have a comprehensive understanding of different aspects, such as the resulting microstructure and the interaction between the laser and the solder material [Jiang, 2021]. Qualitative research has revealed distinct intermetallic compound formations (IMC formations) in laser soldering, which is a contactless method that eliminates the need for hot soldering tips. The characteristics of IMC formation are influenced by various factors, including laser wavelength, power output, pulse duration, and laser beam size [Jiang, 2021]. The formation of IMCs significantly impacts the mechanical properties and quality of solder joints. Two types of IMC formations have been observed: scalloped and prismatic. Scalloped microstructures exhibit refined particles, while prismatic microstructures appear coarse. Solder joints with prismatic IMC formations exhibit higher shear force compared to those with scalloped formations [Jiang, 2021]. The determination of laser parameters that result in either scalloped or prismatic microstructure was achieved using Jackson's parameter [Jiang, 2021].

Numerical analysis conducted by Kunwar (2017) focused on SAC solder paste and compared it to polished microstructure under varying output power and short pulse durations. The

study utilized a high-power laser with a wavelength of 915 nm. The findings indicated that prismatic IMC formations could be produced by moving the laser at low scan speeds along solder substrates with a power output of 30-50 W (wavelength of 1528-1565 nm). This dataset was utilized alongside a Neural Network to predict prismatic formations using Jackson's Parameter [Kunwar, 2020].

In-situ monitoring during the laser soldering process has been achieved through X-ray imaging, allowing researchers to observe the morphological changes over time [Ma, 2013]. Comparative studies conducted by Tatsumi (2022) compared the impact properties of solder and microstructure using an infrared wavelength laser and a blue light laser. The study varied power and pulse durations on a fixed-size joint and found that the efficiency and impact properties were significantly better under blue light due to higher absorption (23% increase compared to IR) [Tatsumi, 2022].

A notable aspect to consider regarding laser-material interaction is the monitoring of electrical resistance throughout various stages of joint creation, subsequent process steps involving thermal changes, and the overall lifecycle of the joints. To evaluate the reliability of solder joints under thermo-mechanical cycling, four-wire resistance measurements have been conducted to assess high resistances [Duan, 2014]. This study demonstrates a hybrid AM approach that combines material extrusion AM, ultrasonic wire embedding, micro-dispensing of solder paste, and laser soldering to create electrical joints. As part of the process development, in-process resistance measurements were performed across the fabricated joints too characterize their behavior and guide further improvements. This approach was developed to identify the specific process step responsible for joint failure when issues such as high resistance or lack of continuity were observed. The focus was particularly on understanding the thermal history and resistance response during thermal events in the fabrication process, such as laser soldering and encapsulation with heated thermoplastic material.

## Materials and Methodology

### Coupon Fabrication

Testing coupons were produced using the Foundry Multi$^{3D}$ System, as described in previous work [Billah, 2019]. The system comprised wo Fortus 400mc material extrusion AM machines from Stratasys, Inc. (Eden Prairie, MN, USA) and a modified LC 3024 Computer Numeric Control (CNC) system from Techno CNC (Ronkonkoma, NY, USA, equipped to support machining, ultrasonic wire embedding, solder paste dispensing, and laser soldering. The fabrication process followed the following sequence: 1) A polycarbonate (PC) base was 3D printed, 2) a cavity for the connector and a channel for wires were machined into the base, 3) copper wires were ultrasonically embedded into the base, 4) excess wire was machined to the desired length, 5) the connector was placed into the cavity, 6) solder paste was dispensed at the joint, 7) the joint was soldered using laser technology, 8) the area around the connector and atop the PC base was 3D printed to create a cavity, 9) epoxy was dispensed into the created cavity, and 10) the entire PC area, including the epoxy-filled cavity, was 3D printed over.

The design of the coupon consisted of a rectangular prism base measuring 35 x 21 x 3.65 mm, featuring a cavity for a 527450697 connector from Molex (Lisle, IL, USA) and channels for bare copper wires with a diameter of 34-gauge (ø = 0.1601 mm), as shown in Figure 1. The connector used was a six-pin Easy-on FFC/FPC connector with a pitch of 250 microns and leads

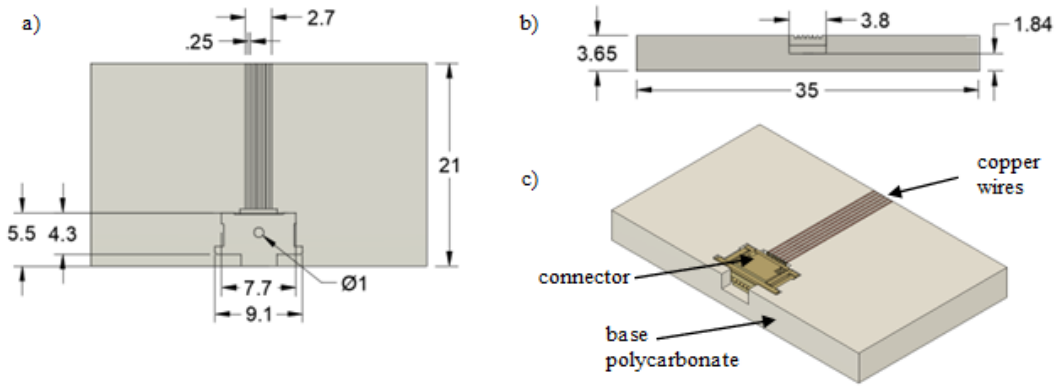


Figure 1. CAD designs (all dimensions in mm). a) Top view of the machined specimen. b) Front view. c) Isometric view of coupon with copper wires and Molex connector.

of 200 microns in width. The base was initially 3D printed using PC and then machined to create precise mating features for the connector and wires. An ultrasonic sonotrode was employed to embed the wires into their respective channels. Excess wire measuring 9-14 mm was used to create free leads opposite the connector. The copper wire ends were utilized for resistance measurements, with an expected resistance range of 20.6-25.3 mΩ. During ultrasonic wire embedding, the kinetic energy generated by the sonotrode impaled the wire into the PC material and produced localized heat at the work area. However, the desired level of heating was carefully controlled to ensure that the embedding process occurred in a solid state. This limited heat input and the solid-state nature of ultrasonic wire embedding are considered advantageous for on-orbit manufacturing, as the influence of gravity is minimal and excessive heat can have negative effects.

Inside the connector, a separate insertable flexible flat cable of flexible printed circuit (FFC/FPC) was inserted, featuring six leads on the opposite end corresponding to the FFC ribbon. One end of the ribbon was soldered with a 152.4 mm long 24-gauge copper wire to the lead of the connector was measured and found to be approximately 38.6 mΩ. Without solder, the total resistance range was between 59.2-63.9 mΩ. To dispense the solder paste, a Type IV, Sn96.5-Ag3-Cu0.5 solder paste from Nordson (Westlake, OH, USA) was used. The dispensing was carried out by a 7194 Auger style pump, equipped with a 25-gauge needle. The needle was manually positioned at the appropriate connector lead relative to the tip of the leads, with the assistance of a CMOS camera.

**Four-Wire Resistance Measurements and Visual Observations**

During the process of laser soldering, two CMOS cameras from Basler AG (Ahrensburg, Germany, Europe) and a BK-2841 DC resistance meter from BK Precision (Yorba Linda, CA, USA) were utilized for targeting, solder reflow observations, and four-wire resistance measurements, respectively. To prevent oversaturation from laser light during soldering, the camera used for in-process observations was equipped with a filter. The resistance meter emphasized an accuracy of 0.01% and a resolution of 0.01 μΩ, capable of measuring resistance within the range of 2-200 mΩ (with a maximum output of 5V and 1A at this range). The resistance meter formed a circuit that incorporated the copper wire, solder joint, connector, and ribbon cable in series, shown in Figure 2. To ensure the proper positioning and stability of the connector, Thermoplastic Polyurethane (TPU) was extruded, acting as a physical constraint in case the cavity did not provide a perfect fit or in the event of movement caused by the resistance meter probes.

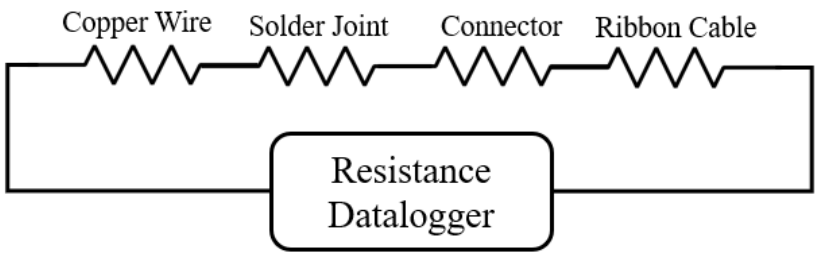


Figure 2. Setup for resistance measurements during laser soldering.

## Laser Soldering

A programmable semiconductor diode laser with a wavelength of 808 nm, manufactured by NaKu Technology, Co., Zhejiang, China, was utilized in conjunction with a LabVIEW virtual instrument (VI) from National Instruments in Austin, TX, USA. The laser operation followed a specific power profile: 1) Initially, it operated at 2 W until the user corrected the laser position. 2) Then, it gradually ramped up from 2 W to 3.4 W over a span of 15 seconds to induce solder reflow. 3) Subsequently, it ramped down from 3.4 W to 2 W over 15 seconds to allow for solidification. 4) Finally, at the end of the laser soldering process, the laser power was set to 0 W. The laser beam was directed to the tip of the Molex connector lead, with half of the laser spot targeting the copper wire and the other half focused on the lead itself. To ensure synchronization between the laser heating and cooling phases, the resistance meter was triggered to start recording data once the targeting was completed. Laser soldering is particularly advantageous in on-orbit manufacturing scenarios, as it does not require physical contact, thus reducing the potential impact of gravity effects or extreme reactions to physical forces.

## Encapsulation

Following the soldering process, the resistances of all leads were documented at the ambient temperature of the room, which was 23°C. After that, additional PC material was extruded over the embedded wires while forming a cavity measuring 9.97 x 8.125 x 1.27 mm (as shown in Figure 4) to accommodate manually dispensed epoxy material. The top of the coupon was completely covered in a final printing step. To facilitate resistance measurement, the exposed copper wires of the coupon were soldered onto an insulated wire that extended outside the printer,

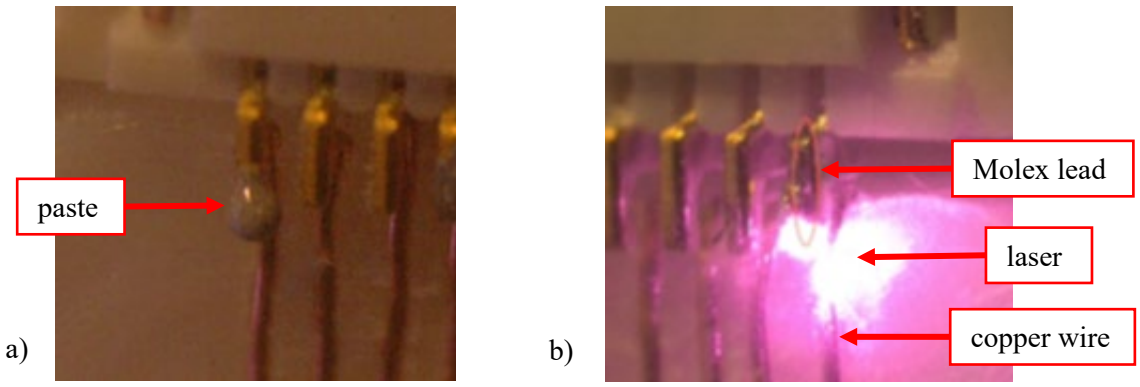


Figure 3. a) Solder paste dispensing, and b) laser soldering.

resulting in an increase of approximately 63 mΩ from the initial temperature reading. The additional wire leads were used to minimize fatigue in the coupon's wire leads and ensure that resistance values remained within the 2-200 mΩ range to maintain consistent accuracy. Prior to encapsulation, a single soldered wire was randomly selected and measured during the encapsulation process. Resistance measurements were recorded for 10 joints. The entire encapsulation process was recorded on camera to identify any potential causes of failure during the printing process. After the complete fabrication process, the coupon was allowed to cool down to room temperature over a period of 24 hours. Resistance measurements were then taken to compare against the measurements obtained prior to printing the encapsulation layers. The resistance reading were captured two minutes after clamping the probes in place.

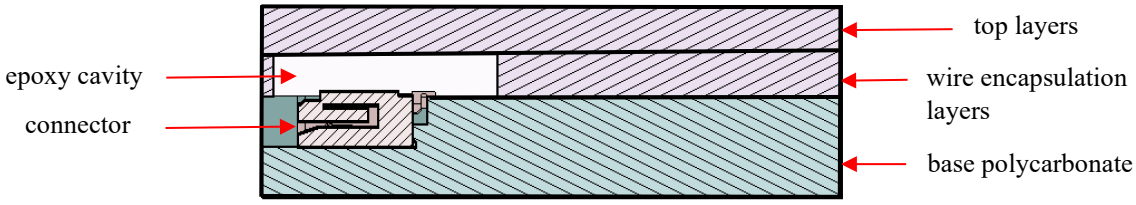


Figure 4. Cross-sectional view of coupon highlighting printing sequences: 1) base polycarbonate, 2) wire encapsulation layers, and 3) top layers.

After the completion of the fabrication process, the coupon underwent a 24-hour cooling period to reach room temperature. Resistance measurements were then conducted to compare them with the measurements obtained prior to printing the encapsulation layers. The measurements were taken two minutes after the probes were clamped.

A separate coupon, identical to the one being tested, was also subjected to temperature and resistance measurements before being hand soldered. For these measurements, a DAQ module 9214 from National Instruments in Austin, TX, USA, was employed along with an E-type thermocouple. The thermocouple was encapsulated in epoxy material directly above the solder joint. Temperature and resistance measurements were captured during the "full encapsulation" phase, while the printer was printing over the epoxy cavity. The objective was to analyze the thermal profile and assess the impact of temperature on resistance.

## Results and Discussion

Out of the 60 connector leads that underwent laser soldering, 48 were successfully connected to copper wire and showed electrical continuity after a single exposure to laser energy. An additional 10 joints required a second exposure to the laser to achieve continuity. In this setup, the desired range for a "good" joint was between 58-65 mΩ. Among the joints created on the first attempt, 45 of them fell within this range, while 8 joints went outside the range due to bridging. However, 6 of those bridge joints were subsequently fixed. After the encapsulation process, a total of 41 joints fell outside the desired range. Following the encapsulation of the 58 joints, 7 wire leads broke, and 4 other leads showed no continuity, resulting in 47 remaining leads for comparison to the pre-encapsulation state. Out of these 47 leads, 34 leads experienced an increase in resistance by 3.83%, with a standard deviation of 4.13%. On the other hand, 13 leads experienced a decrease in resistance by -3.77%, with a standard deviation of 5.49%.

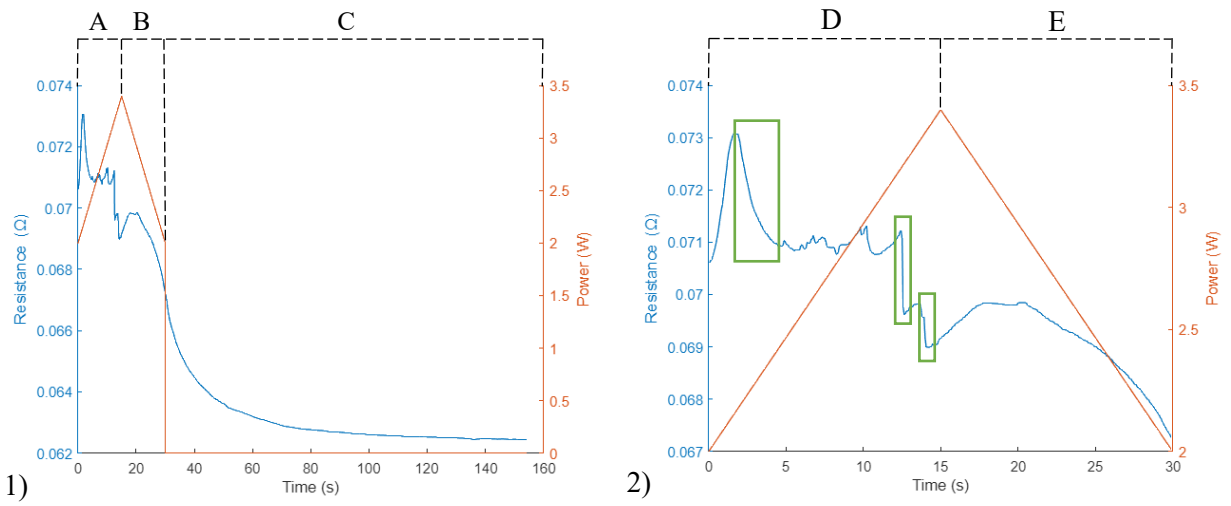


Figure 5. Resistance across a joint of a coupon undergoing laser soldering. 1) full duration where region A represents the laser heating stage from time 0 to 15 seconds, region B represents the laser cooling stage from time 15 to 30 seconds, and region C is environmental cooling beyond 30 seconds. 2) 30-second timeframe where laser is active: region D corresponds to the laser heating stage (t = 0 – 15 s), and region E is laser cooling stage (t = 15 – 30 s). The resistance highlighted in green was measured during the formation of liquid solder, which attached the lead and the wire characterized by drops in resistance. Also, as the solder transitions from a liquid to solid state (t ≈ 22-25 s), the resistance gradually decreased with power.

The joints that successfully connected exhibited an average resistance of 59.93 mΩ with a standard deviation of 6.15 mΩ. Prior to the encapsulation process, 6 joints that had experienced bridging were manually fixed. After encapsulation, the average resistance of the total 47 leads was 61.6 mΩ, with a standard deviation of 4.01 mΩ. The two joints that initially showed no continuity maintained their state after encapsulation, and the two joints that were bridged prior encapsulation remained bridged, as evidenced by their low resistance of less than 55 mΩ.

The following provides a description of characteristics curves illustrating temperature and resistance. These findings are expected to be particularly valuable due to the consideration of using this hybrid AM approach for on-orbit fabrication. The upcoming descriptions and the data represented in Figures 6-7 can serve as a basis for comparison if experiments are conducted under on-orbit conditions. Regarding successful joints achieved through the laser soldering process, the resistance showed the following trends (Figure 5): 1) During the initial 0-7 seconds of increasing heat, leads without initial contact showed continuity or a gradual decrease in resistance as liquid solder formed gradually. 2) Between 7-12 seconds, as the solder reflowed and the laser power (and joint temperature) continued to rise, an increase in resistance was observed. 3) From 12-15 seconds, there was another decline in resistance, indicating the occurrence of wetting between the wire and the lead. 4) Throughout the cooling phase, from 15-30 seconds, the joint's resistance varied as the laser power decreased. 5) Between 30-120 seconds, the resistance gradually decreased until it stabilized at room temperature.

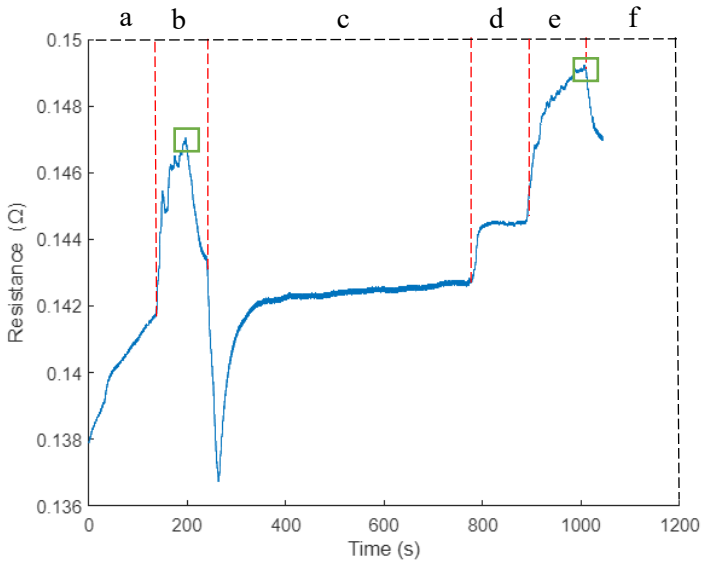


Figure 6. Resistance across a representative joint of a coupon undergoing encapsulation. Region a was the initial heating phase inside the chamber (t = 0 to 170 s), region b occurred when the build plate lifted and started the first part of encapsulation (t = 170 to 240 s), region c was when build plate lowered, the chamber was open, and epoxy was applied on the cavity and left for 10 minutes (t = 240 to 780 s), region d was when the build plate lifted and waited for the nozzle to start printing (t = 780 to 950 s), region e involved the printing process, where the entire coupon, including the epoxy cavity, was encapsulated (t = 950 to 1020 s), and region e represents the cooling phase of the coupon after the encapsulation process (t =1020 s onwards).

After the completion of the coupons' manufacturing and cooling, resistance measurements revealed two observations on the 9 out of 60 joints that experienced failure: ether continuity was absent, or the resistance increased by approximately 10% compared to the stable nominal value. However, none of the resistance measurements taken during the encapsulation process for the 10 coupons indicated such issues. This was primarily due to the uneven heating of the printer and the printing location on the build platform which impacted the wire's heating and prevented the normalization of collected data. Instead, the trends of the measurements were observed as follows (see Figure 6). 1) Initially, when the component was prepared for printing (region a), the lifting of the printing bed caused changes in resistance as the wire configuration shifted and focused heating was applied to the coupon. 2) As the coupon was being printed on (region b), the resistance initially increased until the nozzle printed directly on top of the wire, resulting in a significant rise in resistance. It then decreased (highlighted by a red circle), indicating that the wire was heated by the radiation from the nozzle and the deposited material (T = 345 °C), followed by cooling to the chamber environment (145°C). 3) Opening the chamber door (region c) and dispensing epoxy over the joint led to a decrease in resistance as the fluid was at room temperature, cooling the joint and wire. 4) While the curing process was underway, the resistance increased as the epoxy underwent heating inside the chamber. 5) After a period of 10 minutes had elapsed, the printing bed was lifted, and the wire configuration was different (region d). 6) Significant resistance increases were observed when the nozzle passed through the epoxy (region e).

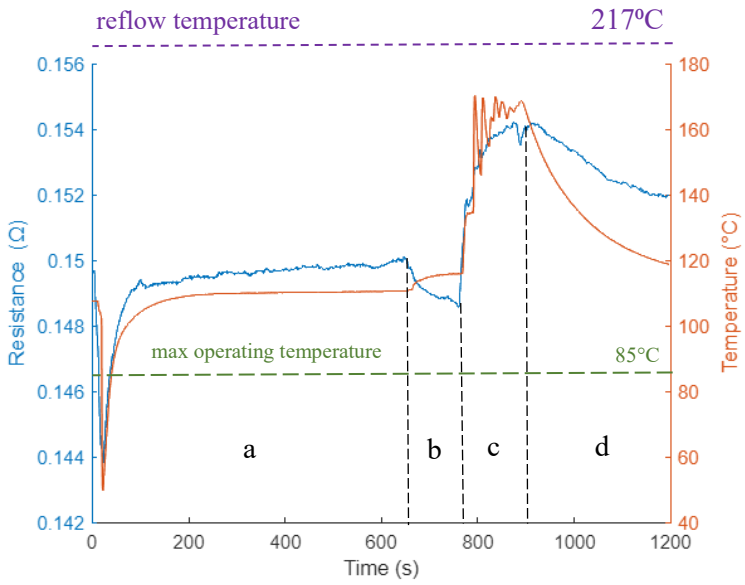


Figure 7. Resistance and temperature profile of a hand-soldered coupon undergoing encapsulation for the whole coupon and cavity. In region a, epoxy was dispensed onto the cavity, followed by curing of approximately 10 minutes (t = 0 to 640 s). In region b, the build plate lifted and prepared for the printing phase (t = 640 to 780s). Region c is when printing started from 780 s to 900 s. Region d is after printing, where temperature decreased with resistance (past 900 s).

During the process of fabricating the epoxy cavity, the average maximum resistance of 10 joints was recorded as 152.6 mΩ, with a standard deviation of 6.66 mΩ. These resistance values are higher compared to previous tests due to the increased length of the wires. It is worth noting the remarkable consistency in resistance measurements among the 10 joints at that particular stage, as indicated by a low coefficient of variation (CV = 0.043). Similar consistency was also observed at the completion of printing (end of region e) with an average resistance (μ) of 157.4 mΩ, a standard deviation (σ) of 15.69 mΩ, and a coefficient of variation of 0.099.

Regarding the resistance and temperature measurements (see Figure 7), the thermocouple recorded a maximum temperature of approximately 170°C, while the maximum resistance reached around 154 mΩ. At this temperature, the solder joint remained in its solid state. However, any potential failures could have been caused by factors such as vibration, temperature variations, or prolonged exposure to temperatures exceeding the connector's maximum operating temperature of 85°C. During this stage, there was no contact between the nozzle and the wires; only vibration occurred due to the rapid movements of the nozzle and the build platform.

## Conclusion

The presented research imparts on the thermal history and resistance behavior of laser soldered joints during their encapsulation using 3D printing. These findings serve as a foundation for future experiments, particularly those conducted under on-orbit conditions. Additionally, this study successfully demonstrated an automated laser soldering solution for fine pitched leads through the implementation of a hybrid additive manufacturing approach for 3D printed electronics. As AM continues to expand its applications in producing innovative devices, this work highlights the integration of multiple technologies, resulting in the creation of coupon-level components that possess physical, mechanical, and electronic functionalities. The ability to achieve multiple functionalities is crucial for various applications that demand space-saving characteristics, such as satellites.

Although the in-situ monitoring method cannot be employed for every solder joint due to its intrusive nature, the methodology presented in this study can be utilized to develop and validate design and process parameters. This includes parameters like epoxy cavity dimensions to minimize undesirable thermal effects, as well as laser power and pulse duration. Additionally, the method proves valuable in identifying the root causes of failure and detecting faulty joints during laser soldering. This enables the opportunity to perform a second laser exposure to repair the joint an enhance overall yield. During the laser soldering process, the resistance profile revealed the following key observations: 1) an increase in the solder's molten volume led to a decrease in resistance, 2) the resistance response indicated successful joint attachment, even if visual evidence was challenging to obtain, 3) substantially high resistance response indicated an unsuccessful joint with no attachment. Regarding the temperature profile during encapsulation, it was observed that the temperature at the joint was lower that the solder reflow temperature. Furthermore, resistance measurements taken during the printing process at both stages exhibited increased resistance as the nozzle passed over the wires across each layer.

## Acknowledgments

The research described here was performed at The University of Texas at El Paso (UTEP) within the W.M. Keck Center for 3D Innovation (Keck Center). The authors are grateful to Andrew J. Hall and Jacob I. Rome from Aerospace Corporation for their guidance and support during this research. Also, the authors thank UTEP students: David A. Sepulveda-Navarrete for assisting with machining parameters, Patrick S. Gutierrez for assisting with ultrasonic wire embedding parameters, and Sebastian Oropeza and Anthony Roldan. The authors are thankful to the support from the Department of Energy National Nuclear Security Administration under Award Number DE-NA0004018.

## References

Anil, Kunwar, "A Data-Driven Framework to Predict the Morphology of Interfacial Cu6Sn5 IMC in SAC/Cu System During Laser Soldering", Journal of Materials Science and Technology (August 2020)

Anil, Kunwar, Shengyan, Shang, Peter, Råback, Yunpeng, Wang, Julien, Givernaud, Jun, Chen, Haitao, Ma, Xuenguan, Song, Ning, Zhao, "Heat and Mass Transfer Effects of Laser Soldering on

Growth Behavior of Interfacial Intermetallic Compounds in Sn/Cu and Sn-3.5Ag0.5/Cu Joints", Microelectronics Reliability (November 2017)

B. H., et al., Lu, et al. "Additive Manufacturing Frontier: 3D Printing Electronics." Opto-Electronic Advances, vol. 1, no. 10, Oct. 2018, pp. 180005.

C., Ladd, et al. "In situ printing of stretchable and durable electronics." Advanced Materials, vol. 28, no. 28, May 2016, pp. 5830-5836.

C. M. Shemelya., "3D Printing Multi-functionality: Embedded RF Antennas and Components," European Conference on Antennas and Propagation (EuCAP) (April 2015)

Doris, Hamill et al., "Space Science and Technology Partnership Forum: Analysis for a Joint Demonstration of High Priority, In-Space Assembly Technology." 2018 AIAA SPACE and Astronautics Forum and Exposition (2018)

Hiraoki, Tatsumi, Hiroshi, Nishikawa, "Highly Efficient Soldering of Sn-Ag-Cu Solder Joints Using Blue Laser", Journal of Manufacturing Processes (August 2022)

H. T., Ma, "In Situ Study of the Real-Time Growth Behavior of Cu6Sn5atthe Sn/Cu Interface During the Soldering Reaction", Elsevier Ltd (October 2013)

J. et al., Liu, "Additive manufacturing of embedded interconnects within a stereolithography fabricated package." Journal of Microelectromechanical Systems, vol. 28, no. 1, Feb. 2019, pp. 70-76.

Jiang, Xudong, Liu, Yueli," Numerical and Experimental Study on Laser Soldering Process of SnAgCu Lead-Free Solder", Materials Chemistry and Physics (July 2021)

Kazi Billah, "Electrical and thermal characterization of 3D printed thermoplastic parts with embedded wires for high current-carrying applications", IEEE (January 2019): Volume 7, Pages 18799-18810

Lynn M., Bowman, Keith W., Belvin, Erik E., Komendera, John T., Dorsey, Bill R., Doggett, "In-Space Assembly Application and Technology for NASA's Future Science Observatory and Platform Missions," Proc. SPIE 10698, Space Telescopes and Instrumentation 2018: Optical, Infrared, and Millimeter Wave, 1069826 (6 July 2018)

Melanie L., Grande, Daniel A., DeLaurentis, "Evaluating Strategies for an On-Orbit Servicing, Assembly, and Manufacturing Platform with System-of-Systems Methodologies," AIAA SciTech Forum (January 2021)

Michael, Greenstein, "Optical Absorption Aspects of Laser Soldering for High Density Interconnects", Applied Optics (November 1968): Vol.28, No.21, Pages 4595-4603

Ning, Duan, "Comparison of In-Situ Measurement Techniques of Solder Joint Reliability Under Thermo-Mechanical Stresses", Microelectronics Reliability (October 2014): Volume 54, Issues 9-10, Page 1753-1757

Shemelya, C, "Multi-Functional 3D Printed and Embedded Sensors for Satellite Qualification Structures," IEEE SENSORS (November 2015)

Xin, Hao, Yu, Xiaoju, Liang, Min, Shemelya, Corey, “3-D Printed Parts for a Multilayer Phased Array Antenna System”, IEEE Antennas and Wireless Propagation Letters (November 2018)